Journal of Alloys and Compounds 509 (2011) 809–812

Contents lists available at ScienceDirect

Journal of Alloys and Compounds

journal homepage: www.elsevier.com/locate/jallcom

Polyacrylamide gel synthesis and photocatalytic performance of $Bi_2Fe_4O_9$ nanoparticles

M. Zhang[a,b], H. Yang[a,b,*], T. Xian[a,b], Z.Q. Wei[b], J.L. Jiang[b], Y.C. Feng[b], X.Q. Liu[c]

[a] State Key Laboratory of Gansu Advanced Non-ferrous Metal Materials, Lanzhou University of Technology, Lanzhou 730050, People's Republic of China
[b] School of Science, Lanzhou University of Technology, Lanzhou 730050, People's Republic of China
[c] Department of Physics, Lanzhou University, Lanzhou 730000, People's Republic of China

ARTICLE INFO

Article history:
Received 9 June 2010
Received in revised form
14 September 2010
Accepted 18 September 2010
Available online 25 September 2010

PACS:
81.07.−b
81.16.−c
81.20.Fw

Keywords:
$Bi_2Fe_4O_9$
Nanoparticles
Polyacrylamide gel
Photocatalytic performance

ABSTRACT

In this report, a polyacrylamide gel route is introduced to synthesize $Bi_2Fe_4O_9$ nanoparticles. It is demonstrated that high-phase-purity $Bi_2Fe_4O_9$ nanoparticles can be prepared using different chelating agents. Interestingly, however, the particle size of the products is found to be dependent on the choice of chelating agent. The use of EDTA as the chelating agent allows the production of $Bi_2Fe_4O_9$ nanopowder with a relatively smaller particle size. The photocatalytic experiments reveal that the as-prepared $Bi_2Fe_4O_9$ nanoparticles possess excellent photocatalytic activity for oxidative decomposition of methyl red under ultraviolet and visible light irradiation. Magnetic hysteresis loop measurement shows that the $Bi_2Fe_4O_9$ nanoparticles exhibit a weak ferromagnetic behavior at room temperature.

1. Introduction

With the increase of environment pollution, semiconductor-based photocatalysis has received growing attention as a promising technology for air and water purification [1,2]. TiO_2 has shown to be a powerful photocatalyst for the oxidative decomposition of numerous organic compounds under ultraviolet (UV) light illumination [3–6]. However, the widespread use of TiO_2 has been hindered since it is active only under UV irradiation (wavelength $\lambda < 390$ nm) due to its wide bandgap (~3.2 eV). In order to efficiently make use of solar energy—an abundant natural resource, which consists largely of visible light, to drive photocatalytic reaction, various methods such as doping [7–9] have been attempted to improve the photocatalytic activity of TiO_2 under visible irradiation. Recently, much work has been concerned with the photocatalysis of other oxide semiconductors like $Bi_2Fe_4O_9$, Bi_6WO_{12}, $CaBi_2O_4$, $LaNiO_3$, and $CuAl_2O_4$ [10–15], which have relatively small bandgaps that are appropriate for the absorption of visible light. Among these oxides, $Bi_2Fe_4O_9$ is also interesting because of its multiferroic nature [16,17], high gas sensitivity [18], and catalytic oxidation of ammonia to NO [19].

The creation of nanostructures is a basic strategy to achieve excellent photocatalytic activity since the photocatalytic reaction occurs dominantly on the catalyst surface [2] and nanostructures can undoubtedly provide a large surface area to volume ratio. Up to now, the preparation of nanostructured $Bi_2Fe_4O_9$ has been mainly based on the hydrothermal process [10,11,20–23], sol–gel template method [24], and molten salt technique [25]. In the aspect of morphology control, the hydrothermal route offers an advantage over other preparation techniques; however, the products obtained from the method tend to have a fairly large particle size, and furthermore a cumbersome abstersion process is generally required to clean out impurities. In this report, we introduce a polyacrylamide gel route to synthesize $Bi_2Fe_4O_9$ nanoparticles. Our recent work has demonstrated that the polyacrylamide gel method allows the production of high-quality nanoparticles with a uniform spherical shape [26–28], and also this method exhibits an excellent capability to create core-shell composite nanoparticles [26]. The photocatalytic activity of $Bi_2Fe_4O_9$ nanoparticles fabricated in the present study has been examined by the photodegradation of methyl red

* Corresponding author at: State Key Laboratory of Gansu Advanced Non-ferrous Metal Materials, Lanzhou University of Technology, Lanzhou 730050, People's Republic of China. Tel.: +86 931 2973783; fax: +86 931 2976040.
E-mail address: hyang@lut.cn (H. Yang).

0925-8388/$ – see front matter © 2010 Elsevier B.V. All rights reserved.
doi:10.1016/j.jallcom.2010.09.097

(MR) under UV and visible light irradiation, and the results reveal a high photocatalytic efficiency.

2. Experimental

According to the formula $Bi_2Fe_4O_9$, stoichiometric amounts of $Bi(NO_3)_3{\cdot}5H_2O$ and $Fe(NO_3)_3{\cdot}9H_2O$ were dissolved into an aqueous nitric acid solution. After the solution was clear and without residue, a stoichiometric amount of chelating agent (ethylenediamine-tetraacetic acid (EDTA) or citric acid) was dissolved in the ratio 1.2:1 respect to the cations (Bi, Fe). Subsequently an appropriate amount of glucose was dissolved (about 20 g in 100 ml). Finally, to the solution were added acrylamide monomers in the ratio 9:1 respect to the cations, followed by adjusting the pH value to 3 by addition of ammonia. Every step mentioned above was accompanied by constant magnetic stirring to make the solution transparent and homogeneous. The resultant solution was heated at 80 °C, and a few minutes later was converted into a deep yellow gel. The gel was dried at 120 °C for 24 h in a thermostat drier. The obtained xerogel was ground into a fine powder in an agate mortar, and then submitted to calcination at 400 °C for 3 h in a tube furnace followed by a thermal treatment at 750 °C for 10 h, finally yielding high-quality $Bi_2Fe_4O_9$ nanoparticles.

The phase purity of the prepared $Bi_2Fe_4O_9$ nanoparticles was examined by X-ray diffraction (XRD) using Cu Kα radiation. The particle morphology was investigated by a scanning electron microscope (SEM). The photocatalytic activity of the products was evaluated by the degradation of MR under irradiation of a 20 W low-pressure mercury lamp (λ = 365 nm) and a 20W tri-phosphor fluorescent lamp (λ ≥ 450 nm). The initial concentration of MR was 25 mg l^{-1} with a catalyst loading of 1.25 mg mL^{-1}. Before illumination, the mixed solution was ultrasonically treated for 15 min in the dark. During the photocatalysis experiment, a small amount of the solution was taken, every 1 h, for examination of the MR concentration. The concentration of MR was determined by measuring the absorbance of the solution (where the catalyst particles were filtered off through a millipore filter paper) at a fixed wavelength of λ = 576 nm using a UV–vis spectrophotometer.

3. Results and discussion

Fig. 1 shows the XRD patterns of $Bi_2Fe_4O_9$ samples prepared separately using EDTA and citric acid as the chelating agent. For both the samples, all the diffraction peaks can be indexed in terms of the orthorhombic structure of $Bi_2Fe_4O_9$ (space group: *Pbam*) with unit-cell constants of $a = 7.969$ Å, $b = 8.449$ Å, and $c = 6.004$ Å, revealing the synthesis of high-phase-purity $Bi_2Fe_4O_9$ via the present polyacrylamide gel method. Interestingly, the grain size of the products is found to be dependent on the choice of chelating agent. The use of EDTA as the chelating agent produces a $Bi_2Fe_4O_9$ sample with relatively broad diffraction peaks compared with the use of citric acid, as can be seen from the enlarged peaks given in the top of Fig. 1. This indicates that $Bi_2Fe_4O_9$ sample with a smaller grain size is readily obtained by using the chelating agent EDTA. Fig. 2(a) and (b) displays the SEM images of $Bi_2Fe_4O_9$ particles prepared, respectively, using EDTA and citric acid as the chelating agent. One can see that the EDTA-based product has an average particle size centered around 200 nm while the citric acid-based product has a particle size centered around 300 nm.

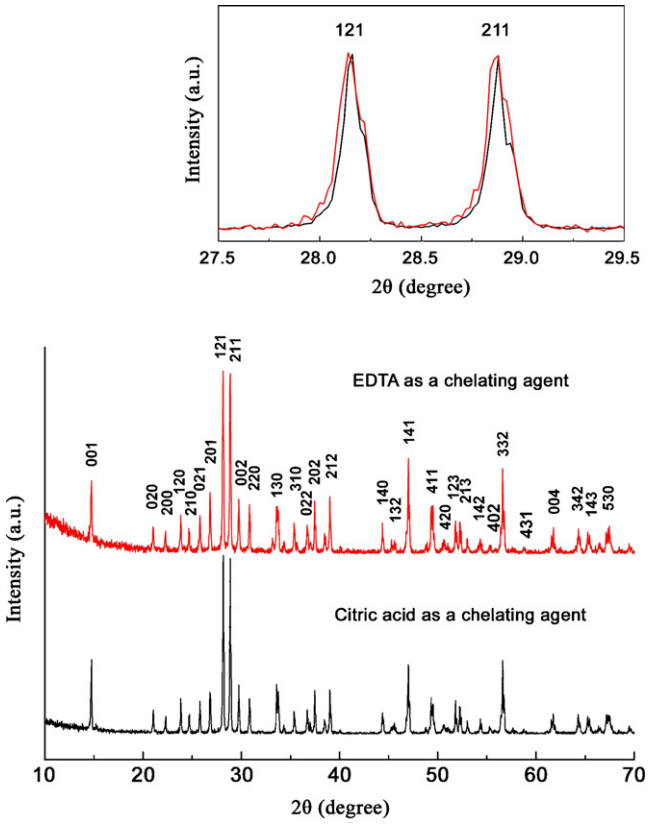

Fig. 1. XRD patterns of $Bi_2Fe_4O_9$ samples prepared separately using EDTA and citric acid as the chelating agent. Shown in the top of the figure is an enlarged view of selected diffraction peaks.

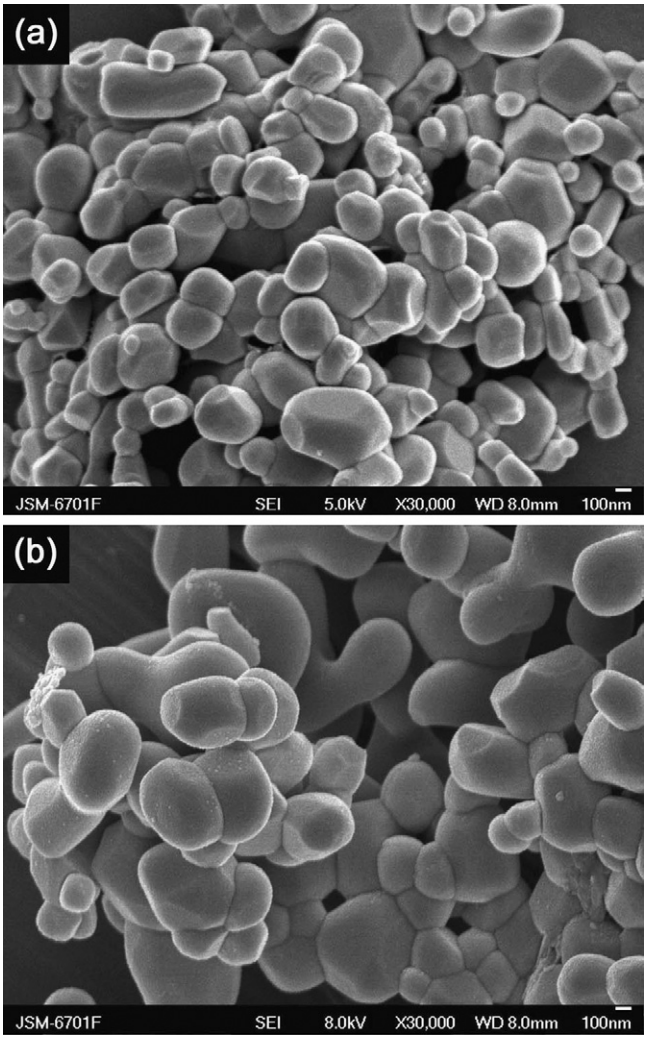

Fig. 2. SEM micrographs of $Bi_2Fe_4O_9$ particles prepared using (a) EDTA and (b) citric acid as the chelating agent.

Fig. 3(a) shows the diffuse reflectance spectra of the $Bi_2Fe_4O_9$ samples measured using a UV–vis spectrometer, and Fig. 3(b) gives the corresponding absorption spectra transformed from the diffuse reflectance spectra according to the Kubelka–Munk (K–M) theory [29]. The energy bandgaps of the $Bi_2Fe_4O_9$ samples can be estimated from the plots of $(\alpha h\nu)^{1/2}$ versus $h\nu$ using the Tauc relation [30], as shown in Fig. 3(c), where α is the K–M absorption coefficient and $h\nu$ is the incident photon energy. The linear portion of the plots is extrapolatted to the $h\nu$ axis to yield the energy bandgap. It is seen

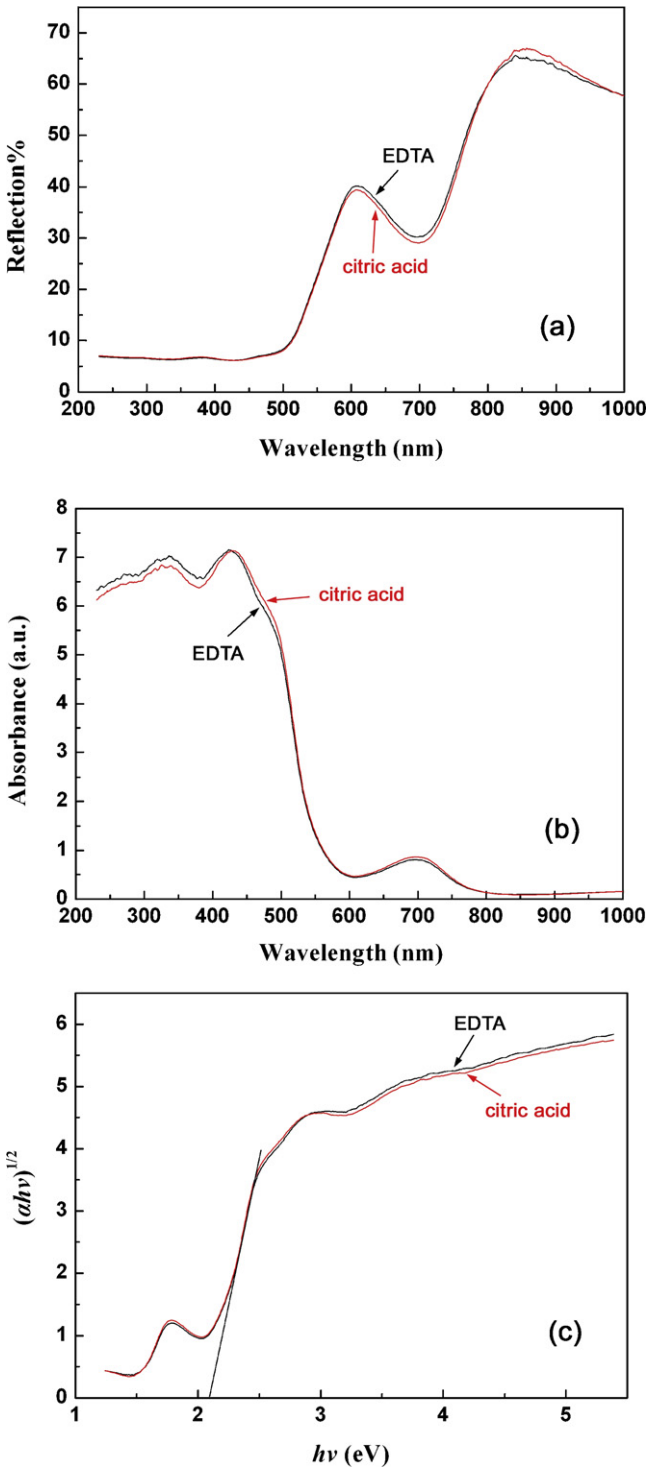

Fig. 3. (a) Diffuse reflectance spectra of the $Bi_2Fe_4O_9$ samples prepared separately using EDTA and citric acid as the chelating agent. (b) The corresponding absorption spectra transformed from the diffuse reflectance spectra according to the K–M theory. (c) The Tauc plots of $(\alpha h\nu)^{1/2}$ versus $h\nu$, where the linear portion is extrapolatted to the $h\nu$ axis to yield the energy bandgap.

that the two samples exhibit a very similar bandgap around 2.08 eV. This value, which is much smaller than that of the famous photocatalyst TiO_2 (~3.2 eV), allows the efficient absorption of visible light.

The photocatalytic activity of the $Bi_2Fe_4O_9$ samples was evaluated by the degradation of MR under UV and visible irradiation. Fig. 4 shows the degradation rate, defined as $(C_0 - C)/C_0 \times 100\%$, as

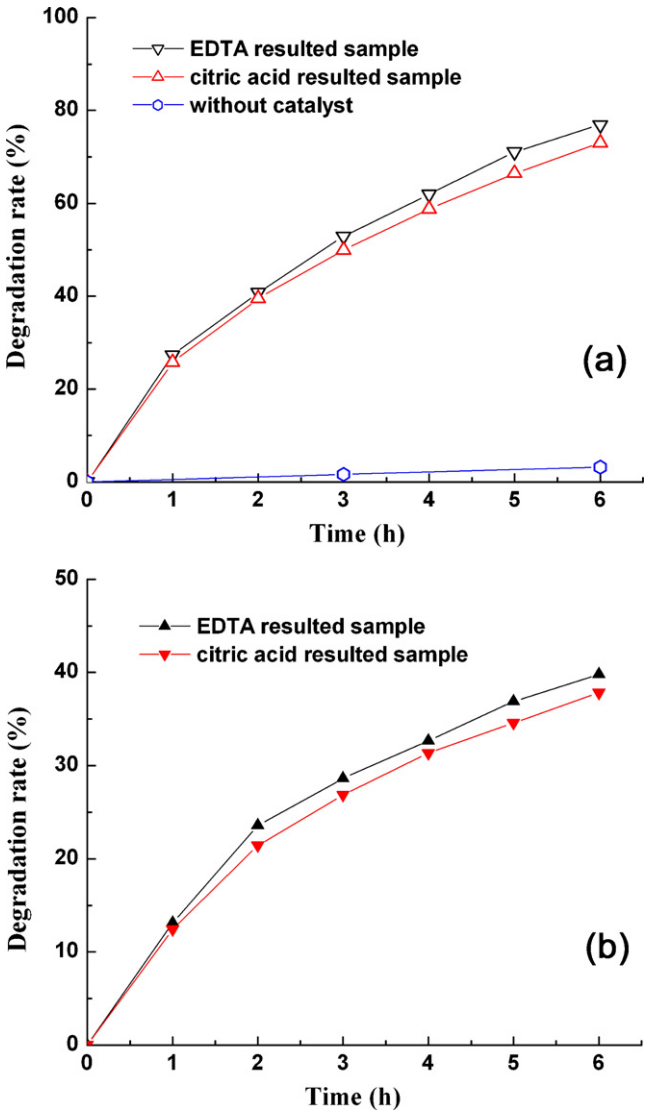

Fig. 4. Photocatalytic degradation of MR as a function of time using the $Bi_2Fe_4O_9$ nanoparticles. (a) Under UV-light illumination; (b) under visible-light illumination.

a function of time, where C_0 and C are the concentrations of MR before and after irradiation, respectively. The methyl red appears to be stable under irradiation without $Bi_2Fe_4O_9$ photocatalyst, and the degradation rate is less than 4% after 6 h UV irradiation. The introduction of $Bi_2Fe_4O_9$ nanoparticles leads to a marked photocatalytic decomposition of the methyl red. It is seen that the $Bi_2Fe_4O_9$ sample prepared using EDTA as the chelating agent exhibits a photocatalytic activity slightly higher than the sample prepared using citric acid as the chelating agent. This can be attributed to its relatively smaller particle size and larger surface area to volume ratio. After 6 h UV irradiation, the MR degradation rate reaches ~77% using the EDTA-resulted sample and ~73% using the citric acid-resulted sample (see Fig. 4(a)). More importantly, the $Bi_2Fe_4O_9$ system exhibits a good visible-light photocatalytic degradation of MR, as demonstrated in Fig. 4(b). After 6 h of visible irradiation with the two samples, the MR degradation rate separately reaches ~40% and ~38%.

Fig. 5 shows the magnetic hysteresis loops for the $Bi_2Fe_4O_9$ samples measured at room temperature, revealing a weak ferromagnetic behavior. For the EDTA-resulted sample, the remanent magnetization (Mr) is ~0.0084 emu/g and the coercivity value Hc is ~200 Oe. For the citric acid-resulted sample, the remanent

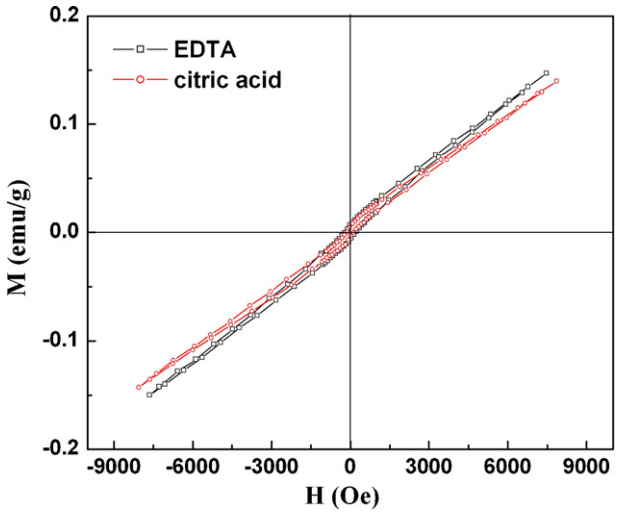

Fig. 5. Magnetic hysteresis loops for the $Bi_2Fe_4O_9$ samples measured at room temperature, revealing a weak ferromagnetic behavior.

magnetization and coercivity are observed to be ~0.0054 emu/g and ~130 Oe, respectively. The origin of weak ferromagnetism in $Bi_2Fe_4O_9$ nanoparticles can be attributed to the surface effects. Generally, in the nanocrystalline system, those physical effects, such as the termination of the crystal structure, lattice distortion, deviation of stoichiometric composition, and dislocation, are expected to become appreciable at the particle surface due to the large surface-to-volume ratio. This leads to the deviation of the surface spins from the antiferromagnetic arrangement, and the macroscopic weak ferromagnetic behavior comes from the disordered surface spins. Similar weak ferromagnetic phenomenon was also observed in other nanosized antiferromagnetic materials, such as $BiFeO_3$ [31] and $Bi_2Mn_4O_{10}$ [32].

4. Conclusions

In this work, we introduce a polyacrylamide gel route to synthesize $Bi_2Fe_4O_9$ nanoparticles. It is demonstrated that this route allows the synthesis of high-purity $Bi_2Fe_4O_9$ nanoparticles using different chelating agents. The particle size of the products is found to have a dependence on the choice of chelating agent, and the use of EDTA as the chelating agent favorably leads to the synthesis of $Bi_2Fe_4O_9$ fine powder having a relatively small particle size. The as-prepared $Bi_2Fe_4O_9$ nanoparticles exhibit an excellent photocatalytic activity for the degradation of methyl red under both UV and visible light irradiation. Magnetic hysteresis loop measurement reveals a weak ferromagnetic behavior in the $Bi_2Fe_4O_9$ nanoparticles at room temperature.

Acknowledgments

This work was supported by the National Natural Science Foundation of China (Grant Nos. 50962009 and 50872047), the key Project of Chinese Ministry of Education (Grant No. 209130) and the Natural Science Foundation of Gansu Province (Grant No. 1010RJZA041).

References

[1] A. Mills, R.H. Davies, D. Worsley, Chem. Soc. Rev. 22 (1993) 417–425.
[2] M.R. Hoffmann, S.T. Martin, W. Choi, D.W. Bahnemannt, Chem. Rev. 95 (1995) 69–96.
[3] D.W. Bahnemannt, S.N. Kholuiskaya, R. Dillert, A.I. Kulak, A.I. Kokorin, Appl. Catal. B: Environ. 36 (2002) 161–169.
[4] S.P. Ruan, F.Q. Wu, T. Zhang, W. Gao, B.K. Xu, M.Y. Zhao, Mater. Chem. Phys. 69 (2001) 7–9.
[5] J.E. Shi, S.X. Shang, L. Yang, J.C. Yan, J. Alloys Compd. 479 (2009) 436–439.
[6] E. Arca, G. Mulas, F. Delogu, J. Rodriguez-Ruiz, S. Palmas, J. Alloys Compd. 477 (2009) 583–587.
[7] R. Asahi, T. Morikawa, T. Ohwaki, K. Aoki, Y. Taga, Science 293 (2001) 269–271.
[8] J.X. Yu, S.W. Liu, Z.L. Xiu, W.N. Yu, G.J. Feng, J. Alloys Compd. 471 (2009) L23–L25.
[9] Z.Q. Liu, Y.C. Wang, W. Chu, Z.H. Li, C.C. Ge, J. Alloys Compd. 501 (2010) 54–59.
[10] Q.J. Ruan, W.D. Zhang, J. Phys. Chem. C 113 (2009) 4168–4173.
[11] S.M. Sun, W.Z. Wang, L. Zhang, M. Shang, J. Phys. Chem. C 113 (2009) 12826–12831.
[12] A.P. Finlayson, V.N. Tsaneva, L. Lyons, M. Clark, B.A. Glowacki, Phys. Status Solidi A 203 (2006) 327–335.
[13] J.W. Tang, Z.G. Zou, J.H. Ye, Angew. Chem., Int. Ed. 43 (2004) 4463–4466.
[14] Y.Y. Li, S.H. Yao, W. Wen, L.H. Xue, Y.W. Yan, J. Alloys Compd. 491 (2010) 560–564.
[15] W.Z. Lv, B. Liu, Q. Qiu, F. Wang, Z.K. Luo, P.X. Zhang, S.H. Wei, J. Alloys Compd. 479 (2009) 480–483.
[16] A.K. Singh, S.D. Kaushik, B. Kumar, P.K. Mishra, A. Venimadhav, V. Siruguri, S. Patnaik, Appl. Phys. Lett. 92 (2008) 132910.
[17] Z.M. Tian, S.L. Yuan, X.L. Wang, X.F. Zheng, S.Y. Yin, C.H. Wang, L. Liu, J.Q. Li, J. Appl. Phys. 106 (2009) 103912.
[18] A.S. Poghossian, H.V. Abovian, P.B. Avakian, S.H. Mkrtchian, V.M. Haroutunian, Sens. Actuators B 4 (1991) 545–549.
[19] N.I. Zakharchenko, Russ. J. Appl. Chem. 73 (2000) 2047–2051.
[20] Y. Xiong, M.Z. Wu, Z.M. Peng, N. Jiang, Q.W. Chen, Chem. Lett. 33 (2004) 502–503.
[21] J.T. Han, Y.H. Huang, R.J. Jia, G.C. Shan, R.Q. Guo, W. Huang, J. Cryst. Growth 294 (2006) 469–473.
[22] J.T. Han, Y.H. Huang, X.J. Wu, C.L. Wu, W. Wei, B. Peng, W. Huang, J.B. Goodenough, Adv. Mater. 18 (2006) 2145–2148.
[23] Y.G. Wang, G. Xu, L.L. Yang, Z.H. Ren, X. Wei, W.J. Weng, P.Y. Du, G. Shen, G.R. Han, Ceram. Int. 35 (2009) 51–53.
[24] Z. Yang, Y. Huang, B. Dong, H.L. Li, S.Q. Shi, J. Solid State Chem. 179 (2006) 3324–3329.
[25] T.J. Park, G.C. Papaefthymiou, A.R. Moodenbaugh, Y.B. Mao, S.S. Wong, J. Mater. Chem. 15 (2005) 2099–2105.
[26] H. Yang, Z.E. Cao, X. Shen, J.L. Jiang, Z.Q. Wei, J.F. Dai, W.J. Feng, Mater. Lett. 63 (2009) 655–657.
[27] T. Xian, H. Yang, X. Shen, J.L. Jiang, Z.Q. Wei, W.J. Feng, J. Alloys Compd. 480 (2009) 889–892.
[28] H. Yang, Z.E. Cao, X. Shen, T. Xian, W.J. Feng, J.L. Jiang, Y.C. Feng, Z.Q. Wei, J.F. Dai, J. Appl. Phys. 106 (2009) 104317.
[29] P. Kubelka, F. Munk, Z. Tech. Phys. 12 (1931) 593–601.
[30] J. Tauc, R. Grigorovici, A. Vancu, Phys. Stat. Sol. 15 (1966) 627–637.
[31] T.J. Park, G.C. Papaefthymiou, A.J. Viescas, A.R. Moodenbaugh, S.S. Wong, Nano Lett. 7 (2007) 766–772.
[32] T. Xian, H. Yang, et al., Size-controlled synthesis and weak ferromagnetism of $Bi_2Mn_4O_{10}$ nanoparticles, unpublished.